Energetics of stalk intermediates in membrane fusion are controlled by lipid composition

Sebastian Aeffner, Tobias Reusch, Britta Weinhausen, and Tim Salditt[1]

Institut für Röntgenphysik, Georg-August-Universität Göttingen, Friedrich-Hund-Platz 1, 37077 Göttingen, Germany

Edited by Axel T. Brunger, Stanford University, Stanford, CA, and approved April 12, 2012 (received for review November 28, 2011)

We have used X-ray diffraction on the rhombohedral phospholipid phase to reconstruct stalk structures in different pure lipids and lipid mixtures with unprecedented resolution, enabling a quantitative analysis of geometry, as well as curvature and hydration energies. Electron density isosurfaces are used to study shape and curvature properties of the bent lipid monolayers. We observe that the stalk structure is highly universal in different lipid systems. The associated curvatures change in a subtle, but systematic fashion upon changes in lipid composition. In addition, we have studied the hydration interaction prior to the transition from the lamellar to the stalk phase. The results indicate that facilitating dehydration is the key to promote stalk formation, which becomes favorable at an approximately constant interbilayer separation of 9.0 ± 0.5 Å for the investigated lipid compositions.

curvature energy | hydration force | lipid bilayer |

Exocytosis, intracellular transport, neurotransmission, fertilization, or viral entry, require that two membranes merge into one. This event, membrane fusion, involves a complex interplay of different membrane lipids, proteins, and water molecules on length scales of few nm. Following the "lipidic pore hypothesis", it is now well accepted that membrane fusion involves a sequence of lipidic nonbilayer intermediates, whose formation is catalyzed and guided by a specialized protein machinery (1, 2). A stage termed "hemifusion" in which the lipids of the outer leaflets of two membrane-enclosed compartments about to fuse can mix, whereas the inner leaflets and the enclosed content remain unaltered (3), has been confirmed by a variety of methods including conical electron tomography (4) and, more indirectly; e.g., by electron spin resonance (5) and fluorescence recovery after photobleaching (6). Studying the fusion of protein-free bilayers of well defined lipid composition can contribute useful insights into the physical principles governing the merger of their more complex biological counterparts and clarify the effect of individual lipid species.

The first connection between two lipid bilayers is the so-called stalk sketched in Fig. 1*A* (7). The proximal lipid monolayers have merged into one strongly curved monolayer, whereas the distal ones are still separated and intact. A persistent problem in membrane biophysics is to determine the precise structure of stalks and the free energy barrier for stalk formation. In a long series of papers (8–16), this determination has been attempted within the framework of the continuum theory of membrane elasticity (17, 18). More recently, with the advent of sufficient computational power, simulations including molecular details have become feasible [e.g. (19, 20) and references therein]. While stalk formation between lipid bilayers in close contact is generally accepted as the initial step in possibly all membrane fusion reactions (7), the subsequent stages from stalk to complete fusion are still debated and different pathways may exist (21).

Complementary to these approaches, experimental data on stalk structure and energy are required. Both for the small length scales involved and the transient nature of the intermediate structures, direct observation of membrane fusion by current microscopy techniques is impossible. Structural insights into the process are therefore hard to gain. The 3D electron density $\rho(\vec{r})$ of many proteins or protein fragments is routinely obtained by protein crystallography, which has become an invaluable standard method in structural biology, even if a multicomponent biological process has to be dissected into the relevant protein players. Lipidic structures can be studied in a similar fashion if they assemble into lipid mesophases. Lamellar phases, for example, are well established as model systems for lipid bilayer structure and interactions (22, 23). The 3D electron density $\rho(\vec{r})$ of stalks can be obtained by X-ray diffraction on the stalk phase of certain phospholipids as pioneered by the group of H.W. Huang (24). By now, this technique is the only viable experimental method which provides access to stalk structure with the required sub-nm resolution. However, data are available only for two pure lipids and with rather moderate resolution so far (24–27), and a further analysis quantifying e.g., the curvatures of the bent lipid monolayers is still lacking.

According to a prevalent and widely used conception based on effective molecular shapes (28), the presence of considerable molar fractions of certain "nonbilayer" lipids such as phosphatidylethanolamines or cholesterol in biological membranes facilitates fusion and promotes stalk formation by virtue of their negative intrinsic curvature [e.g., (29, 30)]. As a prerequisite for stalk formation, close contact between lipid bilayers at the fusion site must be established. Due to repulsive forces between lipid bilayers at short separation distances, usually summarized as the "hydration force" (31–33), this is associated with a considerable energy barrier. In addition to effects on monolayer curvature or lipid packing, changes in lipid composition also affect this "hydration barrier". The precise origin of this barrier is still debated (34–36) and both the ordering of water molecules close to the lipid/water interface (37, 38) as well as thermally excited undulations and molecular protrusions out of the bilayer plane (39, 40) have been used as explanations.

In this paper, we address by experimental means how lipid composition modulates stalk structure and the propensity of lipid bilayers to form stalks. We consider curvature and hydration effects and separate the energetics of stalk formation into two contributions: the hydration barrier for bringing planar and parallel lipid bilayers into close contact, and the bending energy for curving lipid monolayers from the planar state into the highly curved stalk. We have quantified the hydration barrier as a function of lipid composition, and have determined the corresponding critical bilayer separation d_w^* at which stalk formation becomes energetically favorable. Then, by applying and extending the X-ray diffraction methods from ref. 24, we have obtained the

Author contributions: S.A. and T.S. designed research; S.A., T.R., B.W., and T.S. performed research; S.A., T.R., and B.W. contributed new reagents/analytic tools; S.A. analyzed data; and S.A. and T.S. wrote the paper.

The authors declare no conflict of interest.

This article is a PNAS Direct Submission.

Freely available online through the PNAS open access option.

[1]To whom correspondence should be addressed. E-mail: tsaldit@gwdg.de.

See Author Summary on page 9678 (volume 109, number 25).

This article contains supporting information online at www.pnas.org/lookup/suppl/doi:10.1073/pnas.1119442109/-/DCSupplemental.

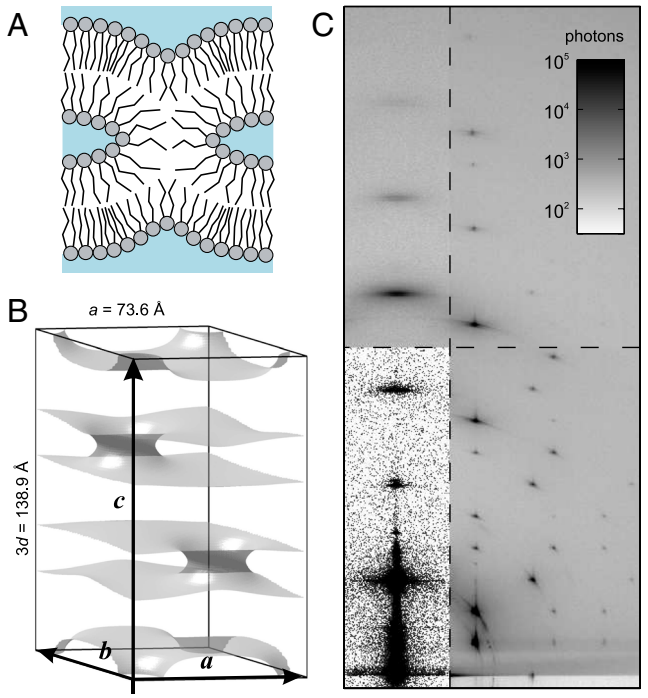

Fig. 1. (*A*) Cartoon of the cross-section of a stalk. (*B*) Arrangement of stalks in the nonprimitive hexagonal unit cell of the stalk phase spanned by vectors $\vec{a} = (a, 0, 0)$, $\vec{b} = (-a/2, \sqrt{3}a/2, 0)$, $\vec{c} = (0, 0, 3d)$. Shown is the electron density isosurface $\Delta\rho = 0.3$ (DOPC/DOPE 1:1, $RH = 74\%$). (*C*) Grazing-incidence X-ray diffraction pattern of the stalk phase (DPhPC, $RH = 70\%$, recorded at the MS beamline, Swiss Light Source) composed of four overlapping Pilatus images. An attenuator with a transmission of 10^{-3} was used in case of the detector position covering primary and specular beam.

structure of stalks in seven different lipid systems, including data on lipid mixtures, with unprecedented resolution. We introduce an approach based on differential geometry of implicit surfaces to analyze lipid monolayer curvature in $\rho(\vec{r})$. Surfaces requiring a minimum amount of bending are found by using the integrated squared mean curvature as the objective function. This method allows a direct comparison of monolayer curvature based exclusively on experimental data. The results are further analyzed within the framework of the continuum theory of membrane bending.

Complementary to the tremendous progress in simulations of membrane fusion in recent years, as well as in the understanding of the protein machinery involved, our work elucidates the structural rearrangements of the lipid matrix at the fusion site by experimental means. Our work aims to provide insights into the conditions which must be established and the work that needs to be performed by fusion proteins in vivo, and allows an estimation of the involved free energy differences based on structural data.

Results

Phase Diagrams and Existence of Stable Stalk Phases. As a prerequisite for the structural analysis reported here, the phase diagrams of lipid model systems forming the stalk phase of rhombohedral symmetry (R) were required, as a function of the main control parameter relative humidity (RH) and lipid composition. Note that the present study focuses on stable stalk phases in thermal equilibrium, while many more systems may display interesting transient or metastable stalk phases. To single out stable stalk phases, we have used own work as well as published data on diphytanoylphosphatidylcholine (DPhPC) and mixtures of dioleoylphosphatidylcholine (DOPC) with dioleoylphosphatidylethanolamine (DOPE) and cholesterol (Chol) (25, 27, 41). In addition, we have detected stable stalk phases in several di-mono-unsaturated phosphatidylcholines, structurally similar to DOPC, but with different chain lengths. The corresponding phase diagram is shown in the *SI Appendix*, Fig. S1. These measurements allow us to study stalks formed between bilayers of different thickness. Addition of nonbilayer lipids such as DOPE and Chol significantly shifts the phase boundary between the lamellar (L) and R phase, promoting stalk formation at higher RH. The used molar fractions of 50 mol% DOPE and up to 30 mol% Chol are close to the maximum amount of these lipids at which the R phase persists in mixtures with DOPC. All lipid systems, along with the respective phase transition values $RH_{L\to R}$ observed in our experiments are listed in Table 1.

Critical Interbilayer Distance for Stalk Formation. In a second step, the lamellar phase of all lipid systems was studied at RH values above and close to the phase transition. The hydration force opposing bilayer approach was quantified by the osmotic stress method in conjunction with electron density profile (EDP) analysis (31, 33, 42). The water layer thickness d_w is defined as the difference of the lamellar repeat spacing d and the distance d_{hh} defined by the position of electron density maxima indicating lipid headgroups (Fig. 2*B*). As demonstrated by model calculations, the positions of these peaks can be determined with an accuracy of 0.1–0.5 Å (44). For all lipids, dehydration was accompanied by a slight increase in d_{hh} (Fig. 2*C*). As described in the *SI Appendix*, the onset of lateral correlations in the lipid bilayer stack is already observed at some percent in RH above the L/R phase transition (*SI Appendix*, Fig. S4). From the corresponding EDPs, we infer that stalk phase formation is initiated at an approximately constant bilayer separation of $d_w^* = 9.0 \pm 0.5$ Å, independent of lipid composition and the associated hydration force parameters and phase transition value $RH_{L\to R}$.

Table 1. Summary of results on bilayer repulsion and stalk curvature in several lipid systems

		Bilayer repulsion (lamellar phase)				Curvature analysis (stalk phase)			
Lipid or lipid mixture	$RH_{L\to R}$	$P_0[10^9$ Pa]	λ_h [Å]	W_{hyd} [k_BT]	RH	Σ_1^*	ρ_{iso}^*	Σ_2^*	RH
di14:1PC*	21	4.13 ± 0.38	2.29 ± 0.06	91 ± 25	50–70	3.92 ± 1.31	0.18	139.8 ± 3.0	13–17
di16:1PC*	37	2.62 ± 0.45	2.56 ± 0.12	98 ± 33	50–90	7.18 ± 1.95	0.26	196.0 ± 5.3	18–31
di18:1PC (DOPC)*	43	3.35 ± 0.37	2.35 ± 0.06	84 ± 23	60–95	7.84 ± 0.80	0.28	207.6 ± 4.6	18–34
di18:1PC (DOPC)†						8.57 ± 0.87	0.28	205.2 ± 3.8	24–32
di20:1PC	39	3.19 ± 0.77	2.34 ± 0.14	78 ± 34	50–90	-	-	-	-
DPhPC*	82	0.39 ± 0.04	3.50 ± 0.11	51 ± 11	82–94	11.79 ± 1.17	0.42	233.0 ± 5.2	70–78
DOPC/Chol 90:10†	50	1.57 ± 0.10	2.56 ± 0.04	59 ± 13	67.5–95	14.14 ± 1.63	0.38	262.7 ± 1.2	36–42
DOPC/Chol 80:20	60	1.24 ± 0.09	2.66 ± 0.05	55 ± 12	72.5–95	-	-	-	-
DOPC/Chol 70:30†	66	0.43 ± 0.11	3.22 ± 0.24	42 ± 17	84–95	16.38 ± 2.79	0.30	196.2 ± 3.1	50–60
DOPC/DOPE 75:25	59	0.62 ± 0.07	3.21 ± 0.12	59 ± 14	76–94	-	-	-	-
DOPC/DOPE 50:50*	73	0.24 ± 0.04	3.68 ± 0.23	38 ± 11	85–94	6.81 ± 0.78	0.24	200.5 ± 7.0	68–74

*GIXD data of the stalk phase recorded at Materials Science beamline, Swiss Light Source, and
†at beamline ID01, European Synchrotron Radiation Facility.

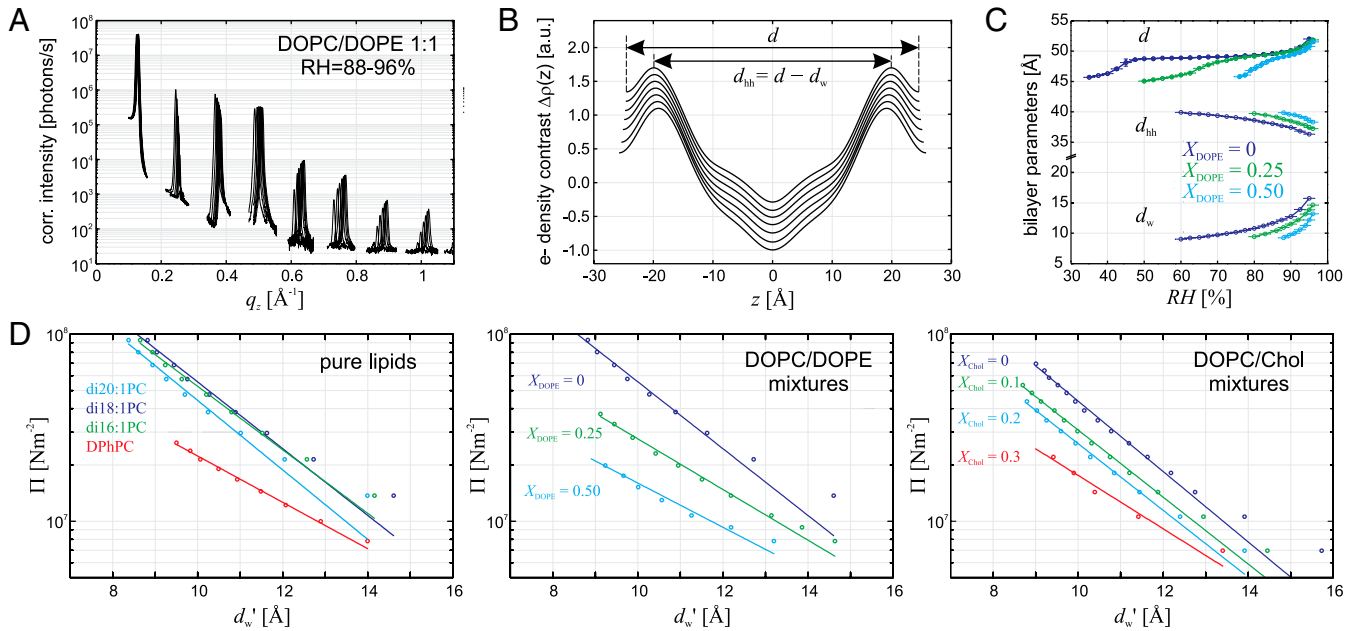

Fig. 2. Bilayer structure and interactions as determined from electron density profiles: (*A*) Typical X-ray reflectivity data indicating eight clearly resolved orders of diffraction, (*B*) corresponding electron density profiles $\Delta\rho(z)$ (shifted vertically for clarity) reconstructed by aid of the swelling method, (*C*) structural data d,d_{hh},d_w for DOPC/DOPE mixtures and (*D*) pressure-distance curves of all investigated lipids. The hydration properties of the branched-chain lipid DPhPC clearly deviate from those of di-monounsaturated PC lipids. Addition of DOPE or cholesterol facilitates dehydration and therefore close bilayer contact. For all investigated samples, stalk phase formation becomes favorable at $d_w < 9.0 \pm 0.5$ Å. In case of DOPC, curves $\Pi(d_w)$ from two independent measurements are shown.

Energy Required for Dehydration. The obtained pressure vs. distance curves $\Pi(d_w)$ in the lamellar state (Fig. 2*D*) were fitted by an exponential decay, yielding the amplitude P_0 and decay length λ_h of the hydration pressure $P(d_w) = P_0 \exp(-d_w/\lambda_h)$ as empirical fit parameters (Table 1). For lower osmotic pressure Π, the bilayer separation d_w tends toward larger values, which could be due to an increase of bilayer undulations (33). The area under each curve between a given value d_w and infinity, $\lambda_h P_0 \exp(-d_w/\lambda_h)$, yields an estimate for the energy (per unit area) required for dehydration up to this point for the particular lipid composition (11). A lower bound for the contact area of two merging bilayers is the cross-sectional area of a stalk, for which we obtain a typical value of $A_s = \pi d_s^2/4 = 20$ nm^2 (see below). The corresponding energies for dehydration W_{hyd} are given for each lipid composition and $d_w = d_w^*$ in Table 1. Values for the di-monounsaturated lipids of different chain length agree within error intervals, while DPhPC, despite its identical headgroup, is substantially easier to dehydrate. The effect of cholesterol and phosphatidylethanolamine lipids was studied by successive addition to DOPC as a host lipid. Both additives systematically reduce W_{hyd} by more than 50% for the highest concentrations used. To obtain the energy for dehydration to form a stalk between planar bilayers such as in the stalk phase, a typical area of $\sqrt{3}a^2/2 \approx 40$–50 nm^2 has to be used; i.e., the values in Table 1 have to be multiplied by a factor of 2–2.5. For example, we obtain $173 \pm 47\ k_BT$ for pure DOPC and $89 \pm 26\ k_BT$ for DOPC/DOPE (1:1 mol:mol). The lattice constant $a \approx 7$ nm (for exact values, see *SI Appendix*) denotes the distance between adjacent stalks in the stalk phase. In summary, the critical interbilayer separation of $d_w^* \approx 9.0 \pm 0.5$ Å for stalk formation is approximately identical for all systems, but the amount of work required to establish d_w^* is not. In particular, addition of the nonbilayer lipids DOPE or Chol considerably reduces its value by up to approximately 50% for the used concentrations.

3D Electron Density Distribution and Stalk Geometry. We have obtained the structures of stalks in seven different lipid systems and lipid mixtures by X-ray diffraction using a modification of the methods introduced by Yang, et al. (25). For each dataset, we observed between 26 and 37 independent reflections and solved the phase problem of crystallography by the swelling method for the rhombohedral phase (25) and additional criteria as described in *SI Appendix*. For further analysis and comparison, we used 25–26 independent reflections whose phases could be unambiguously determined for all samples. This number is higher than in previous datasets on DOPC and DPhPC (24–27) and thus allows a more precise reconstruction of the stalk phase. The spatial arrangement of stalks can be most easily visualized by using a nonprimitive hexagonal unit cell (Fig. 1*A*). Fig. 3*A* displays 2D electron density maps normalized to $\max \Delta\rho(\vec{r}) = 1$ for slices through single stalks. In contrast to conventional crystallography, lipidic structures lack fixed atomic positions and are characterized by thermal disorder and fluctuations (44). Therefore, they are represented by smooth continuous electron density distributions with limited resolution compared to e.g., protein crystallography. Regions of elevated electron density contrast indicate lipid headgroup regions. These regions are separated by regions of lower or negative electron density contrast indicating acyl chains or residual water. Stalks with a strongly curved *cis* monolayer and well separated distal monolayers can readily be recognized. Because diffraction averages over an enormous number of unit cells, the obtained structures are excellent representations of the mean stalk shape for each lipid composition.

By the naked eye, the structures shown in Fig. 3*A* look very similar. The structures also display a very high similarity with the stalk observed in a recent coarse-grained MD simulation by Smirnova, et al. (Fig. 3*B*) (46). In case of DPhPC, the dimples of the *trans* monolayers seem to be slightly more pronounced than in case of the other lipids, however, compared to stalk structures obtained by theory (11–14), they are rather weak. For further analysis and to quantify possible changes, we use the contours of maximum electron density contrast to define the four structural parameters d_s,d_t,d_b,d_w as shown in Fig. 4*A*. In the *xy* plane, the variation of the stalk waist diameter d_s as a function of the polar angle ϕ is typically below 1 Å, and the mean value is used. d_t denotes the distance of the *trans* monolayers, and d_w and d_b

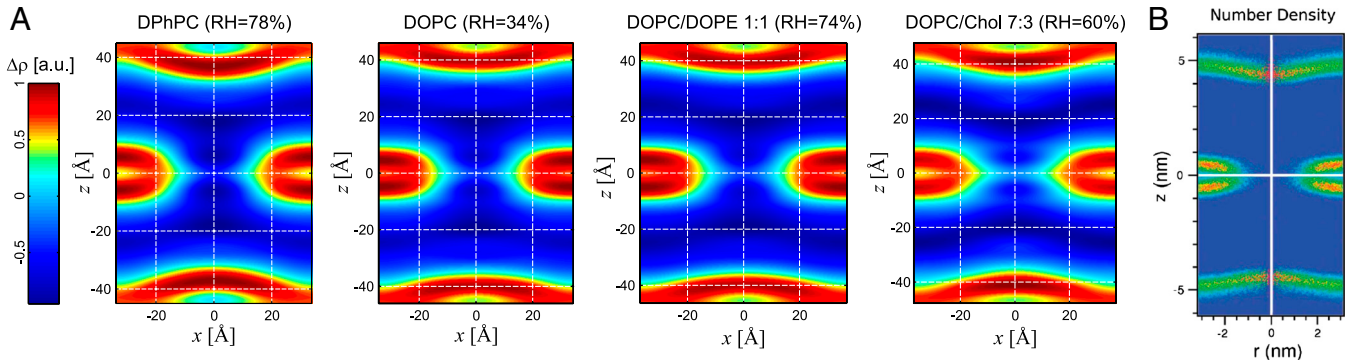

Fig. 3. Side-by-side comparison of different stalks: (*A*) Slices through the *xz* plane of a stalk in different lipid systems. The colorbar applies to all four density maps. (*B*) The density map obtained by a recent MD simulation using POPC (46) shows a very similar stalk architecture. Shown is the lipid headgroup number density. Fig. 3*B* adapted with permission from ref. 46. Copyright (2010) American Chemical Society.

the water layer and bilayer thickness in the stalk phase, respectively.

The results and corresponding dimensionless ratios are summarized in Fig. 4*B* and confirm the visual impression of Fig. 3*A*: The dimensionless ratios of structural parameters display very similar values for all investigated lipids. The overall structure of stalks is therefore highly conserved, with only subtle variations upon addition of the nonbilayer lipids DOPE or Chol or changes in acyl chain length. For each lipid, the four structural parameters as well as the lattice constants *a*,*d* (provided in *SI Appendix*) decrease slightly upon dehydration. Changes in a are significantly stronger than simultaneous ones in d. For the dimensionless ratio d_s/d_b, we find values of $1.13 < d_s/d_b < 1.33$; i.e., the stalk waist diameter is slightly larger than the bilayer thickness. In most samples, the water layer thickness d_w in the stalk phase exceeds the critical value of about $d_w^* = 9.0 \pm 0.5$ Å for transition from the lamellar to the stalk phase (Fig. 4*B*). Formation of the stalk phase is thus associated with a spatial redistribution of the volumes occupied lipid and water which reduces the hydration repulsion at least in a part of the unit cell. This effect is most pronounced in DPhPC, which is also reflected in a lower electron density contrast $\Delta\rho$ close to $(x, z) = (\pm\frac{a}{2}, 0)$ in the density maps in Fig. 3*A*. Addition of cholesterol or DOPE leads to a slight increase of d_w in the stalk phase.

Analysis of Lipid Monolayer Curvature and Bending Energy. In the continuum theory of membrane elasticity, each lipid monolayer of given composition is treated as a homogeneous sheet characterized by few material constants. Bending deformations are described in terms of the two principal curvatures c_1, c_2 or, equivalently, by the mean curvature $H = (c_1 + c_2)/2$ and Gaussian curvature $K = c_1 \cdot c_2$, in each point of the neutral surface (47). This neutral surface applies to the widely used model introduced by Helfrich (18) as well as to extensions including lipid tilt as an additional degree of freedom (47, 48) or higher-order terms in the principal curvatures (49).

To apply this formalism to stalks reconstructed from diffraction data, a reasonable criterion for putative neutral surfaces in electron density representation is required. In lipid bilayers, the neutral surface of each monolayer is usually assumed in the interfacial region between lipid headgroups and acyl chains at a fixed distance from the bilayer center (13). The neutral surface

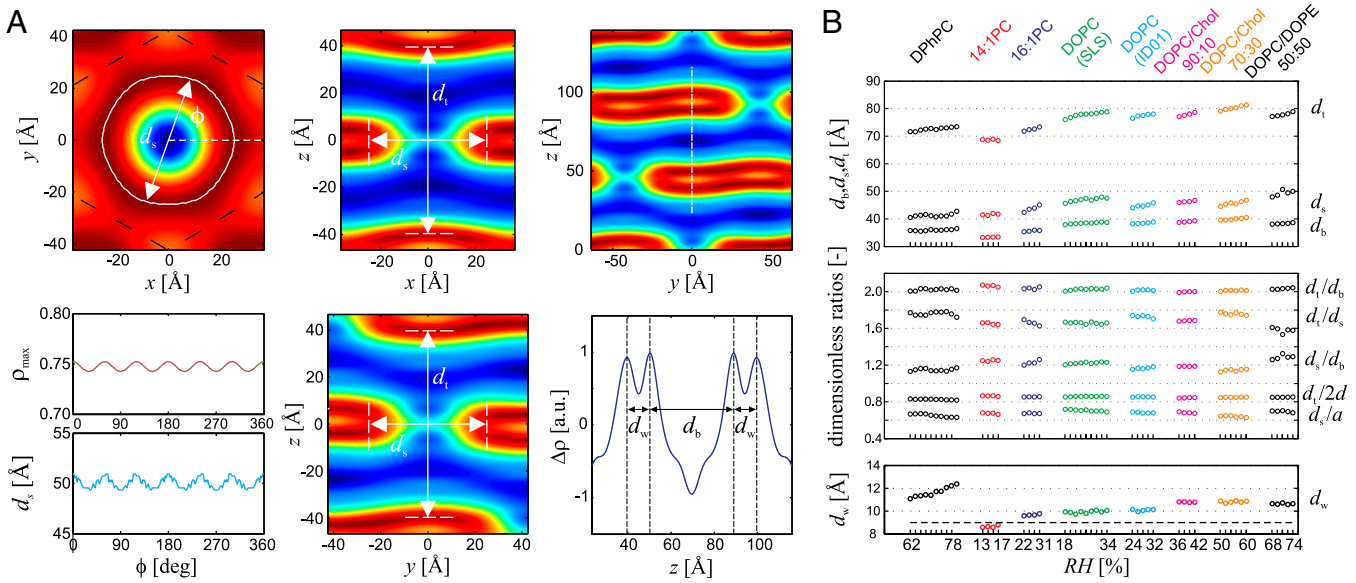

Fig. 4. Quantitative analysis of the stalk phase: (*A*) Definition of structural parameters by local electron density maxima: Electron density contrast $\Delta\rho(\vec{r})$ in the *xy* plane and corresponding stalk waist diameter d_s and maximum electron density contrast (*left*), slices through a stalk in the *xz* and *yz* plane (*center*) and slice through the stalk phase in the *yz* plane and electron density along the white line in vertical direction (*right*) (DOPC/DOPE 1:1, $RH = 74\%$). (*B*) Summary of results for eight different datasets. In the bottom box, the dashed line indicates the value $d_w^* \approx 9$ Å, at which the transition from the lamellar to the rhombohedral phase starts. For most lipid compositions, formation of the stalk phase is associated with an increase of d_w.

corresponds to a certain electron density value within the 1D EDP of the lamellar phase. Therefore, also in the rhombohedral phase, we use surfaces of constant electron density contrast $\Delta\rho(\vec{r}) = \rho_{iso}$, so-called isosurfaces, as approximations to the neutral surface. Of course, the precise choice of an isosurface as an approximation to the neutral surface is debatable. We therefore adapted a strategy of parallelized analysis. The mathematical background and detailed derivations are provided in *Materials and Methods* and *SI Appendix*. Starting from the experimentally determined 3D electron density contrast $\Delta\rho(\vec{r})$, we computed isosurfaces for a range of choices of the parameter ρ_{iso}, followed by a curvature analysis of this entire family of surfaces. Fig. 5 shows typical results: Electron density isosurfaces (Fig.5*A*) and corresponding distributions of c_1,c_2,H and K (Fig. 5*C*) were computed for $\rho_{iso} \in [-0.2, +0.8]$ in steps of 0.02. In this interval, isosurfaces display a stalk-like topology. The threefold rotational symmetry due to the space group $R\bar{3}$ (25) is clearly visible in each plot. At most positions, the two principal curvatures c_1, c_2 are different in sign. The principal curvatures adopt large absolute values in a narrow region close to the stalk waist at $z = 0$. The same applies to the mean and Gaussian curvatures H and K.

Using the Helfrich Hamiltonian, the bending energy difference of the *cis* monolayer of a stalk with respect to a flat monolayer of the same area can be written as $\Delta F_{bend} = \kappa(\Sigma_1 + c_0\Sigma_2) - 4\pi\kappa_G$. Here, $\Sigma_1 = 2A\langle H^2\rangle$ and $\Sigma_2 = -2A\langle H\rangle$ correspond to the squared mean and mean curvature, averaged over the entire monolayer area A. In other words, up to the bending rigidity κ as a prefactor, Σ_1 quantifies the stalk shape in terms of average mean curvature, and Σ_2 quantifies the correction in case the spontaneous curvature c_0 is nonzero for the given lipid composition. The term $\kappa_G\int KdA = -4\pi\kappa_G$ resulting from the Gaussian curvature is a topological invariant due to the Gauss-Bonnet theorem (16).

Fig. 5*D* shows the corresponding curvature integrals Σ_1,Σ_2,A and $\int KdA$ as a function of ρ_{iso} for DOPC and DOPE 1:1, plots of $\Sigma_{1,2}$ for the other lipids are provided in *SI Appendix*, Fig. S6. For fixed ρ_{iso}, Σ_1 and Σ_2 did not vary significantly with RH. We therefore use the averages over all RH levels within the stalk phase of each lipid composition for further analysis and comparison. Solid and dashed lines indicate the corresponding mean and standard deviation. Σ_1 adopts its minimum Σ_1^* for $\rho_{iso} \approx 0.2$–0.4, which corresponds to the interfacial region between lipid headgroups and hydrocarbon region in EDPs of the lamellar phase (Fig. 2*B*). Therefore, we use these Σ_1^* minimizing the average mean curvature for further comparison. The isosurface area A varies monotonously with ρ_{iso}, as expected based on the corresponding shift from the center of the stalk. In contrast to the mean curvature integrals $\Sigma_{1,2}$, A also exhibits a systematic shift

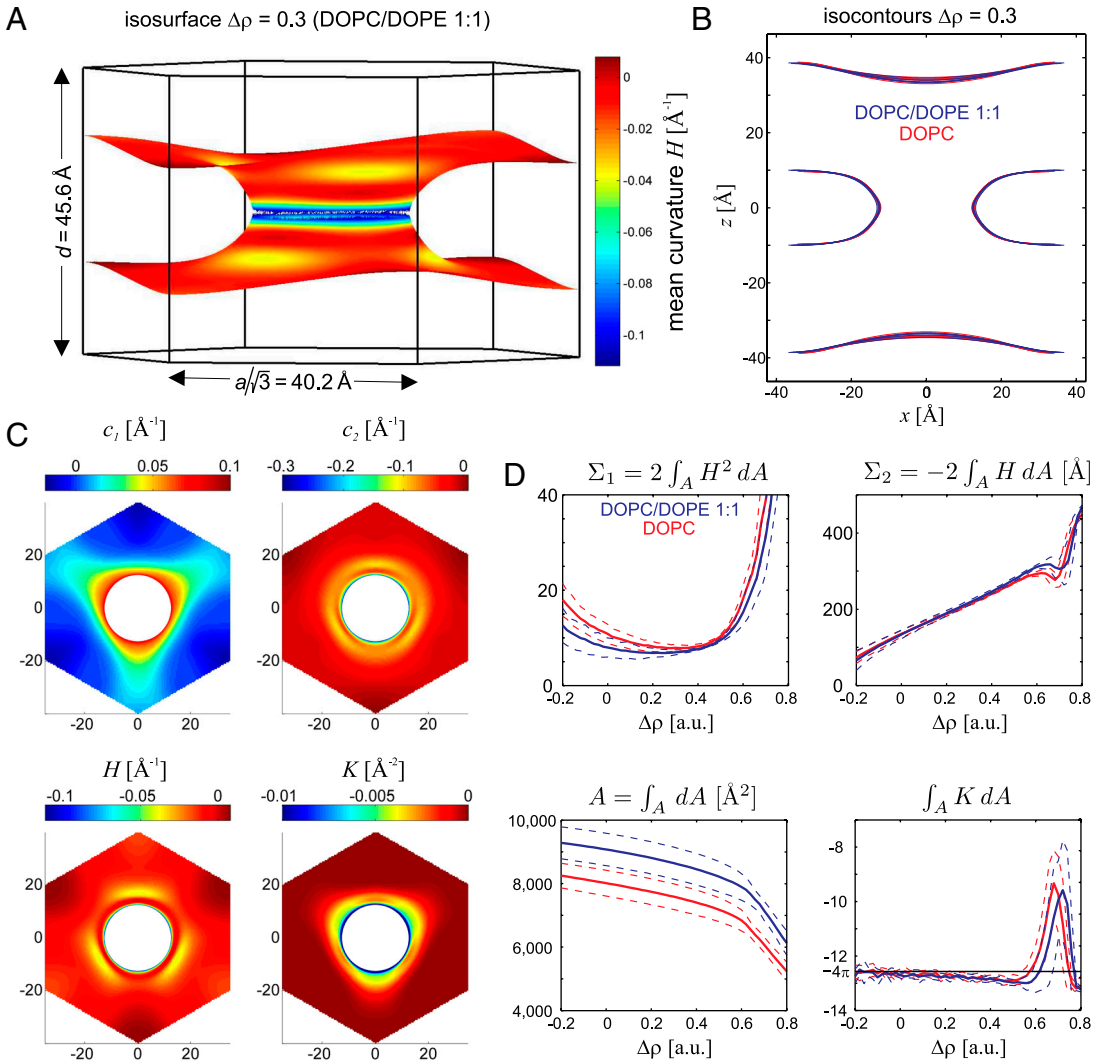

Fig. 5. Evaluation of lipid monolayer curvature by electron density isosurface analysis: (*A*) Electron density isosurface $\Delta\rho(\vec{r}) = 0.3$ for DOPC/DOPE 1:1 ($RH = 70\%$). (*B*) Isocontours $\Delta\rho = 0.3$ at different hydration levels for stalks formed by pure DOPC and DOPC/DOPE 1:1 indicating a very similar structure. (*C*) Principle curvatures $c_{1,2}$, mean curvature H and Gaussian curvature K for $\Delta\rho(\vec{r}) = 0.3$ (top view) and (*D*) results of the integrals Σ_1, Σ_2, A, $\int KdA$.

with RH encompassed within the dashed lines shown in Fig. 5*D*, due to the shrinking/swelling of the unit cell upon changes in lipid hydration. For $\rho_{iso} \leq 0.5$, the numerical results for $\int_A KdA$ are close to the theoretical value -4π expected for the topology of a smooth stalk between planar bilayers (16). In this range of ρ_{iso}, all electron density isosurfaces possess a topology similar to the one in Fig. 5*A*. We use this integral as a control that the algorithm works correctly and attribute residual deviations from -4π to imperfect integration close to $z = 0$ where K assumes its most extreme values.

In case of DOPC, the two datasets containing grazing-incidence data recorded at different synchrotrons agree within error bars. Comparing different lipid compositions, we observe that the minimum value Σ_1^* increases with chain length (i.e., for the lipids di14:1PC, di16:1PC and di18:1PC) and with Chol concentration in DOPC/Chol samples (Table 1). Therefore, longer acyl chains or increased Chol content seem to lead to more strongly curved monolayers. Addition of DOPE to DOPC, on the contrary, does not have a significant effect: electron density isocontours for pure DOPC and DOPC/DOPE 1:1 almost coincide (Fig. 5*B*), and the values of Σ_1 and Σ_2 agree within error bars for the entire considered ρ_{iso} range (Fig. 5*D*).

Discussion

Prior to stalk formation, the lipid bilayers about to merge must come into close contact. This process is opposed by strong, short-range repulsive forces, summarized as the "hydration force". In the pioneering work of Rand and Parsegian reviewed in refs. 31–33, the hydration force parameters P_0, λ_h of many lipids, including those of DOPC and a 1:3 DOPC/DOPE mixture relevant to the present study, have been obtained by the so-called gravimetric method. Here, only the lamellar repeat spacing d is measured. The water layer thickness d_w is not directly obtained, but deduced from d using the highly simplifying assumption that lipid and water molecules partition into distinct and well defined layers and maintain their molecular volumes in bulk. This assumption excludes a possible intercalation of lipids and water, as well as surface roughness at the molecular level (33). Further sources of errors associated with the gravimetric method derive from the simplified assumption that water and lipid as mixed by macroscopic amounts must partition in strict proportion, excluding water pockets defects and any geometric shapes deviating from idealized multilamellar domains (23, 50). Therefore, no precise value of d_w can be obtained by this method. The strategy chosen here, using electron density profiles reconstructed by aid of the swelling method at hydration levels close to the onset of stalk formation, circumvents these drawbacks: It yields the actual bilayer structure (in terms of electron density) in the hydration range relevant for stalk formation and the corresponding hydration force parameters P_0 and λ_h based on a clear definition of bilayer separation distances d_w. Notably, due to the absence of strong bilayer undulations in dehydrated conditions, our EDPs are typically based on eight orders of diffraction, compared to only four at full hydration (51).

It has been noted earlier that the water layer thickness d_w at given osmotic pressure, as calculated from the gravimetric method can deviate significantly from the measured EDP (31). However, these values are still in use: For example, a recent theoretical analysis based on the early hydration force parameters obtained by the gravimetric method for DOPC and a DOPC/DOPE mixture, predicts considerable variations in the critical water layer thickness d_w^* for stalk formation (36), which is in sharp contrast to the practically constant value d_w^* in our experiments. Even after a compressibility correction to take into account changes of bilayer hydration with hydration, the corrected gravimetric values and our new values based on EDPs show opposing different trends on the hydration force decay length λ_h of DOPC/DOPE mixtures. Furthermore, by the compressibility-corrected gravimetric method, an increase of P_0 by about three orders of magnitude has been reported upon addition of 50 mol% cholesterol to eggPC (31). This increase is in striking contradiction to the observation of decreasing P_0 and slightly increasing λ_h obtained by the EDP method for the same lipid system (52), as well as to the observed decrease of d_w at constant pressure upon addition of cholesterol to DOPC (Fig. 2). EggPC and DOPC are different lipids, of course, nevertheless one would certainly expect the same trend. We believe that these discrepancies are due to the questionable assumptions and experimental difficulties associated with the gravimetric method discussed above. The EDP method, in contrast, yields the actual bilayer structure without any prior assumptions, samples are more easily prepared, and results can directly be compared to MD simulations (53). Therefore, we suggest to use hydration force parameters P_0, λ_h obtained by the EDP method for future studies on hydration effects in membrane fusion.

The osmotic pressures required to induce the stalk phase in pure lipids (Table 1) correlate well with recent values for the cross-sectional area A_L per lipid headgroup at full hydration (54, 55): The larger A_L, the lower the critical osmotic pressure corresponding to $RH_{L\rightarrow R}$. Of the used di-monounsatureted lipids, DOPC has the largest A_L at full hydration (54) and requires least osmotic pressure to form the stalk phase. DPhPC, in turn, has a considerably larger A_L than these lipids (55) and undergoes the $L \rightarrow R$ phase transition at substantially lower pressure. A feasible theory to explain this observation is provided by the electrostatic model of Cevc and Marsh, which predicts proportionality between P_0 and the square of the dipole density in the phospholipid headgroup region (38). Following this picture, spreading PC headgroups apart and increasing A_L; e.g., by adding cholesterol (52, 56) or by applying lateral tension (57) would facilitate dehydration and thus hemifusion by reducing the dipole density. Previous experiments using hydration force data obtained by EDP analysis (58) provide support for this theory, however, an alternative explanation based on hydrogen bonding exists (59).

Our electron density reconstructions of the rhombohedral phase allows a side-by-side comparison of stalks formed by different lipid compositions. The dimensionless ratios of structural parameters show little variations; i.e., the stalk morphology in different lipids is approximately constant. If the effective molecular shape of lipids was the key parameter in stalk formation, one would very likely expect more significant changes in stalk morphology and the dimensionless ratios of structural parameters. Furthermore, our electron density maps of stalks are in strikingly good agreement with the stalk structure obtained in a recent molecular dynamics simulation of a stalk formed between two POPC bilayers by Smirnova, et al. (46) (Fig. 3*B*). Comparing the distribution of water in the lamellar and stalk phase close to the phase transition, and considering the sudden increase of water layer thickness upon stalk formation (Fig. 4*B*) one concludes that lipids can be more favorably hydrated in the stalk geometry. In a highly curved stalk structure, water molecules face lipid headgroups in three rather than only two directions, and thus more headgroups may "benefit" from a given number of hydrating water molecules. Along with the structural constancy in the entry point of the stalk phase at the $L \rightarrow R$ phase transition, these observation of a largely universal stalk structure in different lipid systems point to the fact that the distribution of water is the key to understand the formation of stalks. Loosely speaking, rather than focusing on surfaces minimizing bending energy, which has been the case in early papers on stalk formation, the present structural results point to the dominating role of geometries maximizing hydration. Finally, if the propensity for stalk phase formation was dominated by bending energy, one would expect $RH_{L\rightarrow R}$ to decrease with the hydrocarbon chain length, because κ is expected to increase quadratically with monolayer thickness (60). The lowest value of

$RH_{L\to R}$ for di14:1PC and its nonmonotonous sequence for di14:1PC to di20:1PC, which was confirmed in three repeated measurements including calibration of the *RH* sensor, clearly indicate that this is not the case.

With the introduced formalism of electron density isosurfaces, we are now in a position to quantify lipid monolayer curvature and bending energy based on experimentally obtained stalk structures. The obtained results for the curvature integrals $\Sigma_{1,2}$ are directly based on the diffraction data; i.e., lattice parameters and form factors, without further modeling. For a comparison of our stalk structures to results from continuum theory, we consider the results obtained by Markin and Albanesi using the "standard" Helfrich Hamiltonian and requiring $H = \text{const.}$ (12), and by Kozlovsky and Kozlov using a model including lipid tilt and a nonsmooth neutral surface (13). These two models start from two initially flat bilayers, which is the same initial configuration as in our experiments. Because $\Delta\rho(\vec{r})$ is reconstructed by a Fourier series with a limited number of terms, we obtain smooth isosurfaces with neither discontinuities nor a constant mean curvature. Because the curvatures adopt large absolute values in a narrow region close to the stalk waist (Fig. 5*C*), the Kozlovsky/Kozlov structure better matches with our experimental results.

With known elastic coefficients c_0,κ,κ_G, it is possible to estimate the contributions in the Helfrich bending energy. We consider the case of DOPC and DOPE, because their elastic coefficients are available from the literature. For fixed κ,c_0 taken from ref. 16, a minimum of about 50 k_BT for pure DOPC and about 15 k_BT for DOPC/DOPE (1:1) is obtained for the term $\kappa(\Sigma_1 + c_0\Sigma_2)$ (Fig. 6*A*). If c_0 is allowed to adopt slightly more negative values, which could be a realistic assumption in dehydrated conditions (see below), the mean curvature term can approach negative values (Fig. 6*B*). The Gaussian curvature term $-4\pi\kappa_G$ yielding about 100 k_BT for $\kappa_G \approx -\kappa$ (16) dominates the bending energy ΔF_{bend} or accounts for at least more than one half of it. This conclusion is in qualitative agreement with latest results from continuum theory (15, 16). Notably, the work required for dehydration of the area corresponding to the stalk waist W_{hyd} (Table 1) is similar in magnitude to the total curvature energy and, as proposed in ref. 15, could be released by stalk formation and thus make the stalk phase energetically favorable compared to the lamellar phase. Our results on $\Sigma^*_{1,2}$ given in Table 1 for other lipid compositions can be directly applied if their material parameters κ,κ_G,c_0 become available in future.

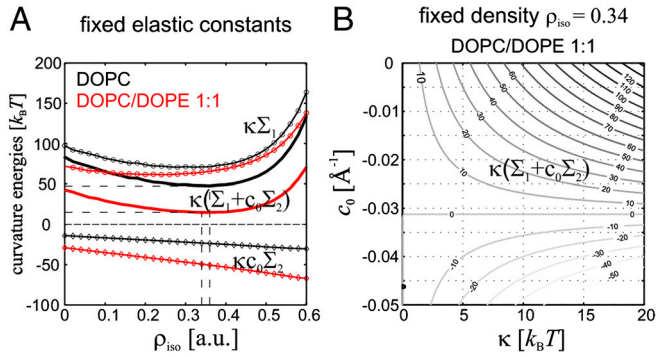

Fig. 6. Combining our structural results with values for bending modulus κ and spontaneous curvature c_0 allows to estimate the bending energy of a stalk: (*A*) Bending energy term $\kappa(\Sigma_1 + c_0\Sigma_2)$ for the case of DOPC ($\kappa = 9\ k_BT$, $c_0 = -0.0115$ Å^{-1}) and an equimolar DOPC/DOPE mixture ($\kappa = 9\ k_BT$, $c_0 = -0.024$ Å^{-1}) as a function of the isodensity value ρ_{iso} The values of κ and c_0 were obtained from (16), in case of the lipid mixture, molar fraction-weighted values are used. (*B*) The same energy for a fixed isosurface (DOPC/DOPE 1:1, $\rho_{iso} = 0.34$) as a function of κ and c_0. If c_0 becomes slightly more negative upon dehydration, as explained in the main text, $\kappa(\Sigma_1 + c_0\Sigma_2)$ may approach negative values.

At this stage, possible limitations should be discussed: The continuum description and the Helfrich Hamiltonian is well accepted if bending deformations are small; i.e., the radii of curvature are large compared to the monolayer thickness. It is debated to what extent this approach and truncating the series expansion of bending energy after quadratic terms in c_1, c_2 are justified and sufficient in case of strongly bent monolayers such as in membrane fusion intermediate structures (12, 13, 46, 57, 61). In addition, as a general concern, it may be doubted if neglecting molecular details is a valid approach on these length scales (57). For example, a locally varying lipid composition and, in case of cholesterol, redistribution between *cis* and *trans* monolayers by lipid flip-flop (62) can not be ruled out. A further issue is the interdependence of lipid headgroup hydration and curvature: At strong dehydration, water molecules are extracted from the first hydration shell directly associated to the lipid headgroups (63). This dehydration could change their effective molecular shape and thus κ,κ_G, and c_0. The expected trends upon dehydration, a more negative c_0 and a less negative κ_G, would both reduce ΔF_{bend} and thus facilitate stalk formation (15). However, we stress that, from an experimental point of view, the dimensionless ratios of structural parameters, as well as the isosurfaces computed from the 3D electron density distribution $\Delta\rho(\vec{r})$ and the associated surface integrals, adequately describe the structure. Of course, molecular configuration and discreteness are important, but for the average stalk structure, the 3D continuum density is a justified and purely data-based description, and thus independent of the validity of continuum elasticity theory. Our structural results lead to curvature integrals which we have formulated free of the elastic coefficients. Future experimental results on the elasticity constants can be directly applied to the structural data deposited here.

It is a frequently encountered inaccuracy that energies obtained by continuum theory; e.g., the value of about 40 k_BT in ref. 13, are interpreted as the total free energy required to induce stalk formation [e.g. (64–66)]. However, this value only includes bending and tilt deformations with respect to a flat monolayer of the same area. The value does not include the Gaussian curvature term and, most importantly, also neglects the energy required for dehydration, which already ranges from about 80 to 250 k_BT for initially flat lipid bilayers and the area of $\sqrt{3}a^2/2$ per stalk in the stalk phase, where stalks are located in close proximity. In simulations of bilayer fusion, two parallel patches of lipid bilayers are usually "prepared" in dehydrated conditions; i.e., at a fixed number of water molecules per lipid molecule well below the one in fully hydrated conditions. Therefore, also here, the free energy cost for stalk formation of 3–15 k_BT obtained by different simulation methods (46, 61, 67) does not include the energy required to establish close bilayer contact, and this hydration barrier based on our results would by far exceed the free energy difference of 3–15 k_BT for the last step from dehydrated bilayers to a stalk. Thus, we believe the present results call for a revision of the current curvature-centered view, and suggest to reinforce work on hydration effects in stalk formation and membrane fusion.

Next, we discuss possible implications of our results for protein-mediated membrane fusion. Both SNARE-mediated and viral (e.g., HIV) membrane fusion involve the formation of helix bundles (68, 69). In case of the formation of a single SNARE complex out of syntaxin, SNAP-25, and synaptobrevin, the 'minimal machinery' required for membrane fusion (70), a free energy release of $\Delta G = 18\ k_BT$ has been measured by isothermal titration calorimetry (65) and $\Delta G = 35\ k_BT$ by surface force apparatus (64), respectively. Based on molecular size, the maximum interaction distance at which the SNARE complex could nucleate is in the range of 5–20 nm (71, 72), which has to be compared to the 0.9 nm of critical distance for hemifusion in our lipid compositions. The short-range repulsive forces that need to be overcome to bring membranes to close proximity prior to fusion are

quantified by the hydration force parameters. Given the decay length λ_h of few Å, integration of the hydration force from 5 or 20 nm to d_w^* yielding the hydration barrier is practically constant. The composition of the involved membranes can significantly affect the required energy: The lipid bilayer matrix of synaptic vesicles contains about 40 mol% cholesterol and a considerable amount of PE lipids (73). For the hydration barrier between a spherical vesicle and a planar bilayer, one obtains $2\pi\lambda_h^2 RP_0 \exp(-d_w^*/\lambda_h)$. With the hydration force parameters of the DOPC/Chol 70:30 mixture (Table 1) and a typical vesicle radius of 20 nm (73), this yields about 84 $k_B T$, and a lower value is expected for the physiological lipid composition. We now postulate that SNARE complex formation may lead to dehydration at the point of contact between the membranes, possibly as a rather 'indirect' effect by SNAREs formation acting at the periphery. It is then reasonable to compare the hydration barrier with the energy release by SNARE formation. The ratio of 2–3 deduced from the above numbers is well compatible with recent observations that 1–3 SNARE complexes are sufficient to achieve membrane fusion (66, 74). In line with the present results, the inhibition of fusion observed after depletion of cholesterol, both in SNARE-mediated (75) and viral fusion (76, 77), as well an increase of the docking efficiency in SNARE-mediated vesicle fusion upon higher PE content (78), may result from the effects of these lipids on the hydration barrier W_{hyd}.

Finally, the present approach may shed some light on the role of charged lipids and ions in hemifusion. It is long known that the interplay of Ca^{2+} and anionic lipids such as phosphatidylserine (PS) facilitates fusion (79–81). This finding has been explained by calcium-induced condensation of charged headgroups and thus phase separation, leading to the formation of hydrophobic defects (82). Our work suggests that the bilayers fuse as soon as the critical separation d_w^* has been induced by Ca^{2+} condensation. Indeed, condensed lamellar phases of anionic lipids are very close to this values: For DOPG/Ca^{2+}, 47 Å d-spacing are reported in ref. 83, which—given the 37 Å bilayer thickness (headgroup-headgroup)—results in a water layer slightly larger than our d_w^*. With additional control parameters (i.e., osmotic pressure, temperatature, composition) a transition to a nonlamellar states is then easily induced. In this context, we also found that the lipid phosphatidylinositol-4,5-bisphosphate (PIP_2), which is enriched at the sites of vesicle fusion of synaptic membranes (84, 85), has a very pronounced effect on the phase behavior of DOPC and promotes stalk and inverted hexagonal phase formation already at concentrations of few mol% (43). As a strongly anionic lipid with three net negative charges, PIP_2 is likely to interact with Ca^{2+}, possibly again facilitating localized dehydration and hydrophobic defect formation. Thus, if proteins induce changes at the plasma membrane that affect ion binding and lipid demixing or repartitioning (cholesterol, PIP_2), this could modify the local membrane hydration and thus modulate synaptic vesicle exocytosis. In this line of argument, the fusiogenic proteins would set a constraint on the interbilayer distance either by directly bringing together opposing bilayers, or indirectly by inducing local dehydration effects through lipid reorganization. In a second step, the induced local dehydration would then lead to stalk formation, not necessarily directly at the protein site (45). The critical value found here for the interbilayer distance $d_w^* \approx 9$ Å (as measured from headgroup to the opposing headgroup) defines the critical value at which the two opposing bilayers relax hydration energy by stalk formation. This distance is possibly required to form lipid bridges, "splay intermediates", where the hydrocarbon tails of a single lipid in one *cis* monolayer insert into the opposing lipid bilayer, as observed in MD simulations (34, 46, 86).

Maybe, the most interesting result of the present study is the predictability of the stalk formation for a given lipid system, based only on hydration force measurements in lipid bilayer stacks. The measured interaction parameters of the hydration force for a given system directly allow for the computation of pressure, work and/or chemical potential at which stalks begin to form, simply by extrapolating the hydration curve to the critical value d_w^*.

Materials and Methods

Additional experimental methods are described in *SI Appendix*.

Sample Preparation and Hydration Control. Oriented lipid bilayer stacks were prepared by deposition of organic lipid solution on cleaned and hydrophilized silicon wafers as a solid support. The samples were placed in environmental chambers with precise relative humidity (*RH*) control, which in turn were mounted on different X-ray diffractometers. $RH = 100\%$ is equivalent to full hydration in aqueous solution (87). Lowering *RH* in a controlled fashion was used to successively extract water molecules from the aqueous layer separating adjacent bilayers. In the investigated phospholipids and mixtures of DOPC/DOPE and DOPC/cholesterol, a phase transition from the lamellar phase to the stalk phase of rhombohedral symmetry could be observed at characteristic and reproducible values $RH_{L\to R}$ given in Table 1. All experiments were carried out at room temperature.

Electron Density Profiles and Bilayer Interactions. X-ray reflectivity scans as described in *SI Appendix* were carried out at different *RH* levels with $\Delta RH = 2$–3% from typically ≥90% down to the stalk phase. In these dehydrated conditions, at least seven lamellar orders of reflection could be recorded for all samples (Fig. 2*A*). At or close to full hydration, this number is typically significantly less. 1D electron density profiles $\Delta\rho(z)$ (Fig. 2*B*) were then reconstructed by aid of the swelling method for lamellar phases described e.g., in ref. 43 and references therein. Following the well established osmotic stress method (31, 33, 42), it is assumed that the total attractive pressure can be approximated by the osmotic pressure $P = -(k_B T/v_w)\ln(RH/100\%)$ which dominates the van der Waals attraction in the used *RH* range (33, 88). Here, v_w denotes the molecular volume of water, k_B Boltzmann's constant and T the absolute temperature. Empirically, the datapoints (d_w,P) are well described by an exponentially decaying function $P(d_w) = P_0 \exp(-d_w/\lambda_h)$ yielding the hydration pressure amplitude P_0 and decay length λ_h as fit parameters.

Reconstruction of Stalk Structure. Reconstruction of the stalk phase was based on the methods described in refs. 24, 25. Due to the unusual 2D powder symmetry of aligned lipid mesophases, different diffraction geometries are required to obtain the form factor amplitudes $|F_{hk\ell}|$ of all observable reflections with Miller indices h, k, ℓ. We used a combination of grazing-incidence X-ray diffraction at two different synchrotron beamlines (ID01, European Synchrotron Radiation Facility, and Material Science beamline, Swiss Light Source), as well as X-ray reflectivity scans and powder diffraction using laboratory diffractometers. The crystallographic phase problem was solved by a combination of the swelling method for the rhombohedral phase (25) and additional criteria based on direct methods of crystallography, as well as the characteristic physico-chemical properties of lipid mesophases, yielding the phase factors $\nu_{hkl} = \pm 1$. A detailed description of the applied protocol, as well as swelling diagrams and tables including all form factors $F_{hk\ell}$ and lattice parameters a,d of the nonprimitive hexagonal unit cell of the rhombohedral lattice (Fig. 1*B*), are provided in *SI Appendix*. Finally, The electron density contrast $\Delta\rho(\vec{r})$; i.e., the deviation from the mean electron density in the unit cell, could be reconstructed on arbitrary scale by the Fourier cosine series

$$\Delta\rho(\vec{r}) = \sum_{h,k,l} \nu_{hk\ell} |F_{hk\ell}| \cos(\vec{q}_{hk\ell} \cdot \vec{r}). \quad [1]$$

Curvature Analysis of Lipid Monolayers. In differential geometry, each point of a smooth and continuous surface embedded in 3D space is characterized by two principal curvatures c_1 and c_2 or, equivalently, mean curvature $H = (c_1 + c_2)/2$ and Gaussian curvature $K = c_1 \cdot c_2$. Using this description, the free energy due to bending deformations can be expanded up to quadratic terms in c_1 and c_2 into the widely used "Helfrich Hamiltonian" (18)

$$F_{bend} = \frac{\kappa}{2} \int_A (2H - c_0)^2 dA + \kappa_G \int_A K dA, \quad [2]$$

where c_0 denotes the spontaneous curvature of a lipid monolayer, κ its bending rigidity and κ_G the Gaussian curvature modulus, all with respect to the neutral surface where energetic contributions due to changes in monolayer curvature and area decouple. For our purposes, we rewrite (Eq. **2**) into the form

$$\Delta F_{\text{bend}} = \kappa(\Sigma_1 + c_0\Sigma_2) - 4\pi\kappa_G \quad [3]$$

denoting the bending energy difference with respect to a flat monolayer of the same area A in terms of the quantities

$$\Sigma_1 = +2\int_A H^2 dA = 2A\langle H^2\rangle_A, \quad [4]$$

$$\Sigma_2 = -2\int_A H dA = -2A\langle H\rangle_A. \quad [5]$$

The expression $\langle\ldots\rangle_A$ denotes the average over the isosurface area A. The term $\kappa_G\int K dA = -4\pi\kappa_G$ independent of the precise stalk shape is due to the Gauss-Bonnet theorem (16). As motivated in the main text, we use electron density isosurfaces $\Delta\rho(\vec{r}) = \text{const.}$ as approximations to possible neutral surfaces in the stalk phase. Due to symmetry reasons, it is sufficient to consider a single *cis* monolayer located in the hexagonal prism indicated in Fig. 5*A*. Within this volume, surfaces of constant electron density contrast $\Delta\rho(\vec{r})$ are given by the implicit equation

$$f(\vec{r}) := \Delta\rho(\vec{r}) - \rho_{\text{iso}} = 0, \quad [6]$$

where ρ_{iso} denotes the chosen isodensity value. At each point $\vec{r}$, the mean and Gaussian curvature of the corresponding isosurface can be determined by the expressions (89–91)

$$H = \frac{\nabla f^T \cdot \text{Hess}(f) \cdot \nabla f - |\nabla f|^2 \cdot \text{Tr}(\text{Hess}(f))}{2|\nabla f|^3}, \quad [7]$$

$$K = \frac{\nabla f^T \cdot \text{Hess}^*(f) \cdot \nabla f}{|\nabla f|^4}. \quad [8]$$

∇f, $\text{Hess}(f)$, and $\text{Hess}^*(f)$ denote gradient, Hessian and adjugate (or classical adjoint) of the Hessian of f. Once H, K are known, the two principal curvatures follow from

$$c_{1,2} = H \pm \sqrt{H^2 - K}. \quad [9]$$

The applied method to extract an isosurface $S_{\text{iso}} = \{\vec{r}|f(\vec{r}, \rho_{\text{iso}}) = 0\}$ from the electron density contrast $\Delta\rho(\vec{r})$ reconstructed by (Eq. **1**), determine H, K at each point of this surface and compute the quantities Σ_1, Σ_2, A, $\int K dA$ is described in detail in *SI Appendix*. An extension to any other functional of c_1,c_2; e.g., Hamiltonians including higher-order terms, is straightforward.

ACKNOWLEDGMENTS. We thank S. Pauli and P.R. Willmott (Materials Science beamline, Swiss Light Source) and G. Carbone and P. Boesecke (beamline ID01, European Synchrotron Radiation Facility) for excellent support and working conditions during the synchrotron experiments. M. Wardetzky (Institut für Numerische und Angewandte Mathematik, Universität Göttingen) is acknowledged for helpful discussions on implicit surfaces. M. Holt (Max-Planck-Institut für biophysikalische Chemie) is acknowledged for helpful discussions on SNARE-mediated membrane fusion. Yuliya Smirnova (Institut für Theoretische Physik, Universität Göttingen) is acknowledged for helpful discussions on simulations of stalks.This work was financially supported by Sonderforschungsbereich 803 "Functionality controlled by organization in and between membranes" funded by Deutsche Forschungsgemeinschaft (DFG). S.A. is supported by a stipend of the Göttingen Graduate School for Neuroscience, Biophysics and Molecular Bioscience (GGNB).

1. Jahn R, Lang T, Südhof TC (2003) Membrane fusion. *Cell* 112:519–533.
2. Martens S, McMahon HT (2008) Mechanisms of membrane fusion: disparate players and common principles. *Nat Rev Mol Cell Biol* 9:543–556.
3. Chernomordik LV, Kozlov MM (2005) Membrane hemifusion: crossing a chasm in two leaps. *Cell* 123:375–382.
4. Zampighi GA, et al. (2006) Conical electron tomography of a chemical synapse: vesicles docked to the active zone are hemi-fused. *Biophys J* 91:2910–2918.
5. Xu Y, Zhang F, Su Z, McNew JA, Shin YK (2005) Hemifusion in SNARE-mediated membrane fusion. *Nat Struct Mol Biol* 12:417–422.
6. Wong JL, Koppel DE, Cowan AE, Wessel GM (2007) Membrane hemifusion is a stable intermediate of exocytosis. *Dev Cell* 12:653–659.
7. Chernomordik LV, Kozlov MM (2008) Mechanics of membrane fusion. *Nat Struct Mol Biol* 15:675–683.
8. Kozlov MM, Markin VS (1983) Possible mechanism of membrane fusion (in Russian). *Biofizika* 28:242–247.
9. Siegel DP (1993) Energetics of intermediates in membrane fusion: comparison of stalk and inverted micellar intermediate mechanisms. *Biophys J* 65:2124–2140.
10. Siegel DP (1999) The modified stalk mechanism of lamellar/inverted phase transitions and its implications for membrane fusion. *Biophys J* 76:291–313.
11. Kuzmin PI, Zimmerberg J, Chizmadzhev YA, Cohen FS (2001) A quantitative model for membrane fusion based on low-energy intermediates. *Proc Nat Acad Sci USA* 98:7235–7240.
12. Markin VS, Albanesi JP (2002) Membrane fusion: stalk model revisited. *Biophys J* 82:693–712.
13. Kozlovsky Y, Kozlov MM (2002) Stalk model of membrane fusion: solution of energy crisis. *Biophys J* 82:882–895.
14. May S (2002) Structure and energy of fusion stalks: the role of membrane edges. *Biophys J* 83:2969–2980.
15. Kozlovsky Y, Efrat A, Siegel DP, Kozlov MM (2004) Stalk phase formation: effects of dehydration and saddle splay modulus. *Biophys J* 87:2508–2521.
16. Siegel DP (2008) The Gaussian curvature elastic energy of intermediates in membrane fusion. *Biophys J* 95:5200–5215.
17. Canham PB (1970) The minimum energy of bending as a possible explanation of the biconcave shape of the human red blood cell. *J Theor Biol* 26:61–81.
18. Helfrich W (1973) Elastic properties of lipid bilayers: theory and possible experiments. *Z Naturforsch* 28:693–703.
19. Marrink S-J, de Vries AH, Tieleman DP (2009) Lipids on the move: simulations of membrane pores, domains, stalks and curves. *Biochim Biophys Acta* 1788:149–168.
20. Shillcock JC, Lipowsky R (2006) The computational route from bilayer membranes to vesicle fusion. *J Phys Condens Mat* 18:S1191–S1219.
21. Schick M (2011) Membrane fusion: the emergence of a new paradigm. *J Stat Phys* 142:1317–1323.
22. Salditt T (2005) Thermal fluctuations and stability of solid-supported lipid membranes. *J Phys Condens Mat* 17:R287–R314.
23. Nagle JF, Tristram-Nagle S (2000) Structure of lipid bilayers. *Biochim Biophys Acta* 1469:159–195.
24. Yang L, Huang HW (2002) Observation of a membrane fusion intermediate structure. *Science* 297:1877–1879.
25. Yang L, Huang HW (2003) A Rhombohedral phase of lipid containing a membrane fusion intermediate structure. *Biophys J* 84:1808–1817.
26. Rappolt M, et al. (2004) Phospholipid mesophases at solid interfaces: in-situ X-ray diffraction and spin-label studies. *Adv Colloid Interfac* 111:63–77.
27. Aeffner S, Reusch T, Weinhausen B, Salditt T (2009) Membrane fusion intermediates and the effect of cholesterol: an in-house X-ray scattering study. *Eur Phys J E* 30:205–214.
28. Israelachvili JN, Marcelja S, Horn RG (1980) Physical principles of membrane organization. *Q Rev Biophys* 13:121–200.
29. Gruner SM (1985) Intrinsic curvature hypothesis for biomembrane lipid composition: a role for nonbilayer lipids. *Proc Natl Acad Sci USA* 82:3665–3669.
30. Churchward MA, et al. (2008) Specific lipids supply critical negative spontaneous curvature—an essential component of native Ca^{2+}-triggered membrane fusion. *Biophys J* 94:3976–3986.
31. Rand RP, Parsegian VA (1989) Hydration forces between phospholipid bilayers. *Biochim Biophys Acta* 988:351–376.
32. Leikin S, Parsegian VA, Rau DC (1993) Hydration forces. *Annu Rev Phys Chem* 44:369–395.
33. McIntosh TJ, Simon SA (1994) Hydration and steric pressures between phospholipid bilayers. *Annu Rev Biophys Biomol Struct* 23:27–51.
34. Gentilcore AN, Michaud-Agrawal N, Crozier PS, Stevens MJ, Woolf TB (2010) Examining the origins of the hydration force between lipid bilayers using all-atom simulations. *J Membr Biol* 235:1–15.
35. Wennerström H, Sparr E (2003) Thermodynamics of membrane lipid hydration. *Pure Appl Chem* 75:905–912.
36. Xu W, Pincet F (2010) Quantification of phase transitions of lipid mixtures from bilayer to nonbilayer structures: model, experimental validation and implication on membrane fusion. *Chem Phys Lipids* 163:280–285.
37. Marcelja S, Radic N (1976) Repulsion of interfaces due to boundary water. *Chem Phys Lett* 42:129–130.
38. Cevc G, Marsh D (1985) Hydration of noncharged lipid bilayer membranes. Theory and experiments with phosphatidylethanolamines. *Biophys J* 47:21–31.
39. Israelachvili JN, Wennerström H (1990) Hydration or steric forces between amphiphilic surfaces? *Langmuir* 6:873–876.
40. Israelachvili JN, Wennerström H (1992) Entropic forces between amphiphilic surfaces in liquids. *J Phys Chem* 96:520–531.
41. Yang L, Ding L, Huang HW (2003) New phases of phospholipids and implications to the membrane fusion problem. *Biochemistry* 42:6631–6635.
42. Parsegian VA, Rand RP, Fuller NL, Rau DC (1986) Osmotic stress for the direct measurement of intermolecular forces. *Methods Enzymol* 127:400–416.
43. Ghosh SK, Aeffner S, Salditt T (2011) Effect of PIP_2 on bilayer structure and phase behavior of DOPC: an x-ray scattering study. *Physical Chemistry and Chemical Physics* 12:2633–2640.
44. Wiener MC, White SH (1991) Fluid bilayer structure determination by the combined use of X-ray and neutron diffraction.I. Fluid bilayer models and the limits of resolution. *Biophys J* 59:162–173.
45. Qian S, Huang HW (2012) A novel phase of compressed bilayers that models the prestalk transition state of membrane fusion. *Biophys J* 102:48–55.

46. Smirnova YG, Marrink S-J, Lipowsky R, Knecht V (2010) Solvent-exposed tails as prestalk transition states for membrane fusion at low hydration. *J Am Chem Soc* 132:6710–6718.
47. Hamm M, Kozlov MM (2000) Elastic energy of tilt and bending of fluid membranes. *Eur Phys J E* 3:323–335.
48. Hamm M, Kozlov MM (1998) Tilt model of inverted amphiphilic mesophases. *Eur Phys J B* 6:519–528.
49. Siegel DP (2010) Fourth-order curvature energy model for the stability of bicontinuous inverted cubic phases in amphiphile-water systems. *Langmuir* 26:8673–8683.
50. Klose G, König B, Meyer HW, Schulze G, Degovics G (1988) Small-angle X-ray scattering and electron microscopy of crude dispersions of swelling lipids and the influence of the morphology on the repeat distance. *Chem Phys Lipids* 47:225–234.
51. Tristram-Nagle S, Petrache HI, Nagle JF (1998) Structure and interactions of fully hydrated dioleoylphosphatidylcholine bilayers. *Biophys J* 75:917–925.
52. McIntosh TJ, Magid AD, Simon SA (1989) Cholesterol modifies the short-range repulsive interactions between phosphatidylcholine membranes. *Biochemistry* 28:17–25.
53. Hub JS, Salditt T, Rheinstädter MC, de Groot BL (2007) Short-range order and collective dynamics of DMPC bilayers: a comparison between molecular dynamics simulations, X-ray, and neutron scattering experiments. *Biophys J* 93:3156–3168.
54. Kucerka N, et al. (2009) Areas of monounsaturated diacylphosphatidylcholines. *Biophys J* 97:1926–1932.
55. Tristram-Nagle S, et al. (2010) Structure and water permeability of fully hydrated diphytanoylPC. *Chem Phys Lipids* 163:630–637.
56. Kucerka N, et al. (2008) The effect of cholesterol on short-and long-chain monounsaturated lipid bilayers as determined by molecular dynamics simulations and X-ray scattering. *Biophys J* 95:2792–2805.
57. Müller M, Katsov K, Schick M (2003) A new mechanism of model membrane fusion determined from monte carlo simulation. *Biophys J* 85:1611–1623.
58. Simon SA, McIntosh TJ (1989) Magnitude of the solvation pressure depends on dipole potential. *Proc Nat Acad Sci USA* 86:9263–9267.
59. Gawrisch K, et al. (1992) Membrane dipole potentials, hydration forces, and the ordering of waters at membrane surfaces. *Biophys J* 61:1213–1223.
60. Marsh D (2006) Elastic curvature constants of lipid monolayers and bilayers. *Chem Phys Lipids* 144:146–159.
61. Katsov K, Müller M, Schick M (2004) Field theoretic study of bilayer membrane fusion. i. hemifusion mechanism. *Biophys J* 87:3277–3290.
62. Bruckner RJ, Mansy SS, Ricardo A, Mahadevan L, Szostak JW (2009) Flip-flop-induced relaxation of bending energy: implications for membrane remodeling. *Biophys J* 97:3113–3122.
63. Hristova K, White SH (1998) Determination of the hydrocarbon core structure of fluid dioleoylphosphocholine (DOPC) bilayers by X-ray diffraction using specific bromination of the double-bonds: effect of hydration. *Biophys J* 74:2419–2433.
64. Li F, et al. (2007) Energetics and dynamics of SNAREpin folding across lipid bilayers. *Nat Struct Mol Biol* 14:890–896.
65. Wiederhold K, Fasshauer D (2009) Is assembly of the SNARE comlex enough to fuel membrane fusion? *J Biol Chem* 284:13143–13152.
66. van den Bogaart G, et al. (2010) One SNARE complex is sufficient for membrane fusion. *Nat Struct Mol Biol* 17:358–364.
67. Norizoe Y, Daoulas KC, Müller M (2010) Measuring excess free energies of self-assembled membrane structures. *Faraday Discuss* 144:369–391.
68. Sutton RB, Fasshauer D, Jahn R, Brunger AT (1998) Crystal structure of a SNARE complex involved in synaptic exocytosis at 2.4 Å resolution. *Nature* 395:347–353.
69. Melikyan GB, et al. (2000) Evidence that the transition of HIV-1 gp41 into a six-helix bundle, not the bundle configuration, induces membrane fusion. *J Cell Biol* 151:413–423.
70. Weber T, et al. (1998) SNAREpins: minimal machinery for membrane fusion. *Cell* 92:759–772.
71. Jahn R, Scheller RH (2006) SNAREs—engines for membrane fusion. *Nat Rev Mol Cell Biol* 7:631–643.
72. Stein A, Weber G, Wahl MC, Jahn R (2009) Helical extension of the neuronal SNARE complex into the membrane. *Nature* 460:525–528.
73. Takamori S, et al. (2006) Molecular anatomy of a trafficking organelle. *Cell* 127:831–846.
74. Mohrmann R, de Wit H, Verhage M, Neher E, Sorensen JB (2010) Fast vesicle fusion in living cells requires at least three SNARE complexes. *Science* 330:502–505.
75. Linetti A, et al. (2009) Cholesterol reduction impairs exocytosis of synaptic vesicles. *J Cell Sci* 123:595–605.
76. Liao Z, Cimakasky LM, Hampton R, Nguyen DH, Hildreth JEK (2001) Lipid rafts and HIV pathogenesis: host membrane cholesterol is required for infection by HIV type 1. *AIDS Res Hum Retrov* 17:1009–1019.
77. Kielian M, Rey FA (2006) Virus membrane-fusion proteins: more than one way to make a hairpin. *Nat Rev Microbiol* 4:67–76.
78. Domanska MK, Kiessling V, Tamm LK (2010) Docking and fast fusion of synaptobrevin vesicles depends on the lipid compositions of the vesicle and the acceptor SNARE complex-containing target membrane. *Biophys J* 99:2936–2946.
79. Akabas MH, Cohen FS, Finkelstein A (1984) Separation of the osmotically driven fusion event from vesicle-planar membrane attachment in a model system for exocytosis. *J Cell Biol* 98:1063–1071.
80. Portis A, Newton C, Pangborn W, Papahadjopoulos D (1979) Studies on the mechanism of membrane fusion: evidence for an intermembrane Ca^{2+}-phospholipid complex, synergism with Mg^{2+}, and inhibition by spectrin. *Biochemistry* 18:780–790.
81. Wilschut J, Papahadjopoulos D (1979) Ca^{2+}-induced fusion of phospholipid vesicles monitored by mixing of aqueous contents. *Nature* 281:690–692.
82. Leckband DE, Helm CA, Israelachvili J (1993) Role of calcium in the adhesion and fusion of bilayers. *Biochemistry* 32:1127–1140.
83. Yaghmur A, Sartori B, Rappolt M (2011) The role of calcium in membrane condensation and spontaneous curvature variations in model lipidic systems. *Phys Chem Chem Phys* 13:3115–3125.
84. Aoyagi K, et al. (2005) The activation of exocytotic sites by the formation of phosphatidylinositol 4,5-bisphosphate microdomains at syntaxin clusters. *J Biol Chem* 280:17346–17352.
85. Chapman ER (2008) How does synaptotagmin trigger neurotransmitter release? *Annu Rev Biochem* 77:615–641.
86. Stevens MJ, Hoh JH, Woolf TB (2003) Insights into the molecular mechanism of membrane fusion from simulation: evidence for the association of splayed tails. *Phys Rev Lett* 91:188102–188105.
87. Katsaras J, Watson MJ (2000) Sample cell capable of 100% relative humidity suitable for X-ray diffraction of aligned lipid multibilayers. *Rev Sci Instrum* 71:1737–1739.
88. LeNeveu DM, Rand RP, Parsegian VA, Gingell D (1977) Measurement and modification of forces between lecithin bilayers. *Biophys J* 18:209–230.
89. Goldman R (2005) Curvature formulas for implicit curves and surfaces. *Comput Aided Geom D* 22:632–658.
90. Gray A (1998) *Modern Differential Geometry of Curves and Surfaces with MATHEMATICA* (CRC Press, FL), 2nd Ed.
91. Spivak M (1975) *A Comprehensive Introduction to Differential Geometry,* (Publish or Perish, Boston), Vol. 3.